

Dual-species stimulated deceleration of MgF molecules with Rb atoms

Jin Wei(魏晋), Di Wu(吴迪), Chenyu Zu(祖晨宇), Yong Xia(夏勇), and Jianping Yin(印建平)
Citation: Chin. Phys. B, 2025, 34 (**7**): 073701. DOI: 10.1088/1674-1056/adcb1f
http://cpb.iphy.ac.cn; http://iopscience.iop.org/cpb

What follows is a list of articles you may be interested in

Sub-Doppler cooling of magnesium fluoride molecules

Jin Wei(魏晋), Di Wu(吴迪), Taojing Dong(董涛晶), Chenyu Zu(祖晨宇), Yong Xia(夏勇), and Jianping Yin(印建平)
Chin. Phys. B, 2025, 34 (**6**): 063701. DOI: 10.1088/1674-1056/adc408

Two types of highly efficient electrostatic traps for single loading or multi-loading of polar molecules

Bin Wei(魏斌), Hengjiao Guo(郭恒娇), Yabing Ji(纪亚兵), Shunyong Hou(侯顺永), Jianping Yin(印建平)
Chin. Phys. B, 2020, 29 (**4**): 043701. DOI: 10.1088/1674-1056/ab7905

Generation of high-energy-resolved NH_3 molecular beam by a Stark decelerator with 179 stages

Bin Wei(魏斌), Shunyong Hou(侯顺永), Hengjiao Guo(郭恒娇), Yabing Ji(纪亚兵), Shengqiang Li(李胜强), Jianping Yin(印建平)
Chin. Phys. B, 2019, 28 (**5**): 053701. DOI: 10.1088/1674-1056/28/5/053701

Effect of external magnetic field on the shift of resonant frequency in photoassociation of ultracold Cs atoms

Pengwei Li(李鹏伟), Yuqing Li(李玉清), Guosheng Feng(冯国胜), Jizhou Wu(武寄洲), Jie Ma(马杰), Liantuan Xiao(肖连团), Suotang Jia(贾锁堂)
Chin. Phys. B, 2019, 28 (**1**): 013702. DOI: 10.1088/1674-1056/28/1/013702

Optical Stark deceleration of neutral molecules from supersonic expansion with a rotating laser beam

Yongcheng Yang(杨永成), Shunyong Hou(侯顺永), Lianzhong Deng(邓联忠)
Chin. Phys. B, 2018, 27 (**5**): 053701. DOI: 10.1088/1674-1056/27/5/053701

Dual-species stimulated deceleration of MgF molecules with Rb atoms

Jin Wei(魏晋)[1], Di Wu(吴迪)[1], Chenyu Zu(祖晨宇)[1], Yong Xia(夏勇)[1,2,3,†], and Jianping Yin(印建平)[1]

[1] *State Key Laboratory of Precision Spectroscopy, School of Physics and Electronic Science, East China Normal University, Shanghai* 200241, *China*

[2] *Collaborative Innovation Center of Extreme Optics, Shanxi University, Taiyuan* 030006, *China*

[3] *NYU-ECNU Institute of Physics at NYU Shanghai, Shanghai* 200062, *China*

(Received 21 February 2025; revised manuscript received 3 April 2025; accepted manuscript online 10 April 2025)

We propose a scheme for dual-species deceleration and trapping of a cold atom–molecule mixture by a frequency chirping stimulated force. We study the stimulated force exerted on MgF and Rb using optical Bloch equations based on a direct numerical solution for the time-dependent density matrix. We analyze the relationship between the frequency chirping rate and the number of MgF molecules and Rb atoms. In addition, we study the dynamical process of molecular deceleration and the effect of transverse diffusion. Monte–Carlo simulations show that buffer-gas-cooled MgF and Rb beams, with initial velocities of 200 m/s and 130 m/s respectively, can be decelerated to less than 10 m/s. This is achieved with laser powers of as low as 357 mW for MgF and 10 mW for Rb per traveling wave. The rapid deceleration minimizes molecular loss due to transverse diffusion during the deceleration process. The estimated number of molecules that can be trapped in a magneto-optical trap (MOT) is about 9.0×10^6, which is an order of magnitude larger than the number of MgF molecules decelerated by the spontaneous radiation force. The results offer a promising starting point for further studies of sympathetic cooling.

Keywords: cold molecule, atomic and molecular mixture, frequency chirping, stimulated force

PACS: 37.10.Mn, 37.10.–x, 37.10.Pq, 33.80.–b

DOI: 10.1088/1674-1056/adcb1f **CSTR:** 32038.14.CPB.adcb1f

1. Introduction

The rich internal degrees of freedom within molecules, such as vibrational and rotational states, provide new pathways for tests of fundamental constants and symmetries.[1–3] Polar molecules, characterized by their anisotropic long-range dipole–dipole interactions, offer novel platforms for studying cold collision chemistry, quantum information encoding and processing, and many-body physics effects.[4–9] Achieving ultracold molecules at lower temperatures and higher densities is certainly of great interest now. In recent years, direct laser cooling techniques have advanced rapidly, enabling magneto-optical trapping (MOT) of diatomic and polyatomic molecules such as SrF, CaF, YO, BaF, and CaOH.[10–15] The blue-detuned optical molasses technology has cooled CaF and SrF to 50 μK,[12,16,17] well below the Doppler limit. Molecules have also been successfully loaded into optical dipole traps, magnetic traps, and optical tweezer arrays.[17–19] The maximum number of molecules trapped in a radio-frequency CaF MOT reaches approximately 10^5.[11]

Current molecular deceleration schemes for magneto-optical trapping rely on the principle of spontaneous radiation force deceleration, using laser frequency sweeping to reduce the longitudinal velocity of molecular beams. However, substantial molecular loss occurs during this process due to extended deceleration distances, complex energy level structures, and dark states, resulting in limited molecule numbers in MOTs.[20–26] The stimulated force deceleration scheme offers a promising solution. When the detuning $\delta > \Gamma$ (spontaneous emission linewidth), the stimulated force ($\hbar k\delta/\pi$) significantly exceeds the spontaneous radiation force ($\hbar k\Gamma/2$). This approach allows for rapid short-distance deceleration of molecules while minimizing transverse diffusion losses during the deceleration process, thus providing a crucial basis for obtaining high-density cold molecular samples.[27–31] Due to the relatively small number of molecules trapped in MOT, conventional cooling methods such as radio-frequency evaporative cooling or optical potential evaporative cooling in optical dipole traps are not conducive to achieving a molecular quantum degenerate gas. Another promising approach is atom–molecule sympathetic cooling, where the first step is to obtain ultracold atom–molecule mixtures. The feasibility of this cooling scheme depends critically on the collisional properties of the atom–molecule pairs, with several candidate species identified[32] and the underlying cooling mechanisms studied in detail.[33] An immediate advantage of atom–molecule co-trapping is the orders of magnitude longer interrogation times compared to molecular crossed beam methods, allowing for the study of cold chemistry, particularly for slow processes.

†Corresponding author. E-mail: yxia@phy.ecnu.edu.cn

© 2025 Chinese Physical Society and IOP Publishing Ltd. All rights, including for text and data mining, AI training, and similar technologies, are reserved.

Research is underway to create cold atom–molecule mixtures. In 2015, Tarbutt's group demonstrated sympathetic cooling of ground-state CaF molecules using ultracold Li and Rb atoms. The molecules were trapped in a microwave trap, while the atoms were trapped in a magnetic trap. Simulations showed that CaF molecules could be sympathetically cooled to 100 μK in about 10 s. By applying evaporative cooling to the atoms, the cooling rate can be increased, allowing the molecules to reach a final temperature of 1 μK within 30 s.[33] In 2017, Akerman *et al.* simultaneously decelerated Li atoms and O_2 molecules to rest in a moving magnetic trap. After deceleration, the mixture was loaded into a static quadrupole trap created by two permanent magnets. They estimated that about 10^9 O_2 molecules and 10^5 Li atoms were captured, with a trap lifetime of about 1 s.[34] In 2018, Morita *et al.* investigated ultracold collisions between spin-polarized SrF ($^2\Sigma^+$) molecules and Rb (^{2}S) atoms, laying the foundation for studying the sympathetic cooling of SrF ($^2\Sigma^+$) molecules in magnetic traps.[35] In 2020, Liu *et al.* proposed a scheme for the simultaneous deceleration of CH_3 and Li atoms using a traveling-wave magnetic decelerator, paving the way for the simultaneous trapping of CH_3 and Li atoms and facilitating sympathetic cooling for the preparation of ultracold radical samples.[36] In 2021, Zhu at Yale University performed experimental optimization of the radio-frequency MOT for Rb atoms in order to achieve sympathetic cooling with SrF molecules.[37] In 2024, Hutzler's group proposed a scheme for sympathetic deceleration and cooling of CH polar molecules using laser-cooled Rydberg atoms in a low-temperature, low-density beam. Their research showed that molecules traveling at a velocity of 100 m/s could be brought to rest within 30 collisions, with minimal inelastic losses.[38]

Indeed, the MgF molecule is a good candidate for laser cooling.[39–46] Here, we propose a scheme that uses the stimulated force to decelerate Rb atoms and MgF molecules, with the goal of producing a cold mixture of Rb atoms and MgF molecules. We theoretically study the stimulated force exerted on MgF and Rb using optical Bloch equations based on a direct numerical solution for the time-dependent density matrix. We show that the frequency chirping method ensures a constant maximum stimulated force on the MgF and Rb during the deceleration process, allowing a sustained interaction between the moving particles and the low-power light. We study the influence of transverse diffusion in the process of stimulated deceleration. This scheme allows more efficient deceleration of atoms and molecules to the MOT capture velocity, allowing atoms and molecules with different masses and properties to be both decelerated and confined in the MOT, which is the starting point for studying atom–molecule collisions under ultracold conditions.

2. Theory and method

2.1. Level structure of MgF and Rb

Figure 1 shows the sketch of the stimulated force on a diatomic molecule and an atom in a π-pulse model,[47] as well as the level structure of MgF molecules and Rb atoms. As shown in Fig. 1(a), the stimulated force is generated by dual-frequency laser beams that propagate in opposite directions, inducing excitation and emission processes in atoms and molecules. The relevant vibrational levels and branching ratios of the X→A transition in MgF molecules are illustrated in Fig. 1(b). The spontaneous emission from $A^2\Pi_{1/2}$ to $X^2\Sigma_{1/2}$ is controlled by the vibrational branching ratio $f_{v'v}$ (the downward orange curve in Fig. 1(b)). Upward solid blue lines denote the transitions driven by lasers $\lambda_{vv'}$. The main cooling transition occurs at a wavelength of $\lambda_{00} = 359$ nm, with a Franck–Condon factor f_{00} of 0.972 for this transition[46] λ_{00} is the main slowing light with a natural linewidth of $\gamma = 2\pi \times 22$ MHz, and the $I_{\rm sat} = 62.5$ mW/cm^2. With the repumping light λ_{10} and λ_{21}, the population accumulating in the vibrational states is repumped back. Figure 1(c) shows the relevant cooling energy levels of a rubidium atom. In 2012, Liebisch *et al.* decelerated an atomic beam of Rb using a stimulated-emission slowing technique that employs a bichromatic standing light wave of high intensity, and increased the atom number in an MOT of low capture velocity by up to a factor of 14, and the load rate into the MOT by a factor of 2.[48] Rb atoms are excited by a 780-nm laser light through the $5\ ^2S_{1/2} \rightarrow 5\ ^2P_{3/2}$ atomic transition for laser cooling, with a natural linewidth of $\gamma = 2\pi \times 6$ MHz, and the $I_{\rm sat} = 3.58$ mW/cm^2.[49]

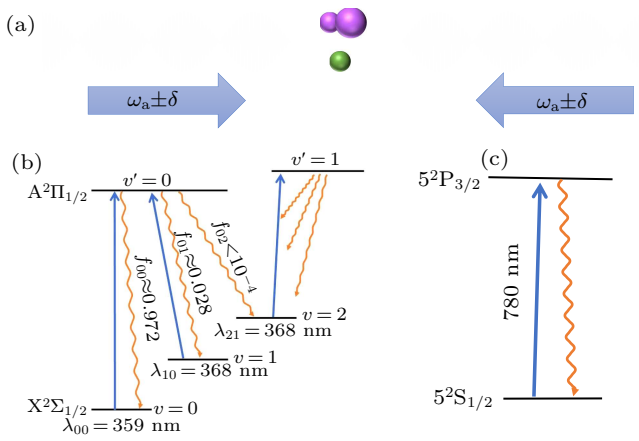


Fig. 1. (a) MgF molecules and Rb atoms in the dual-frequency light field and the light beams are symmetrically detuned by δ from a carrier frequency ω_a. (b) The vibrational energy structure of MgF and the corresponding branching ratios between them. The main cooling transition has $\lambda_{00} = 359$ nm, and the Franck–Condon factor f_{00} for this transition is 0.972. (c) The main energy levels for laser cooling of Rb atoms. The transition wavelength is 780 nm, the upper-state lifetime is 26.24 ns, and the natural linewidth is $2\pi \times 6$ MHz.

We first develop our initial model to calculate the stimulated force on MgF molecules and Rb atoms. In the dual-

frequency light field, the light beams are symmetrically detuned by δ from a carrier frequency $\omega_{\rm a}$, and both frequency components have the same amplitude E_0. The total on-axis electric field is

$$\begin{aligned} E(z,t) &= 2E_0\cos(kz+\omega_{\rm a}t)\cos(\delta t+\varphi/4) \\ &\quad +2E_0\cos(kz-\omega_{\rm a}t)\cos(\delta t-\varphi/4), \end{aligned} \tag{1}$$

where φ is the phase difference between two standing waves, and $k=2\pi/\lambda$. By including the Hamiltonian of the molecules and atoms in the optical field and considering the equation of motion for the density matrix, the optical Bloch equations for the light field can be derived as

$$\dot{\rho} = \frac{[H,\rho]}{{\rm i}\hbar} + L(\rho), \tag{2}$$

where $L(\rho)$ is the Linblad operator to account for spontaneous decay.

We consider the $M_{\rm g}=12+1$ ground states in the MgF molecule. The ground states contain 12 Zeeman sublevels in the $X^2\Sigma^+_{1/2}(v=0,N=1)$ state, and another state includes all other possible vibrational levels as the total population probabilities are equal to 1. There are $M_{\rm e}=4$ excited states in the $A^2\Pi_{1/2}(v'=0,J'=1/2)$ state. The dark states in the ground state $X^2\Sigma_{1/2}(v=0,N=1)$ are destabilized by applying a magnetic field $\boldsymbol{B}$, at an angle θ relative to the laser polarization. Each transition is associated with a Rabi frequency defined by $\Omega^0_{ij}\equiv E_0\cdot d_{ij}/\hbar$, where d_{ij} is the electric-dipole transition matrix element between the states $|i\rangle$ and $|j\rangle$. In the following derivation, the summation over the ground state indices (l, m, n) runs from 1 to 13, while the summation over the excited state indices (i, j, k) runs from 1 to 4. The total Hamiltonian of the system can be expressed as

$$\begin{aligned} H/\hbar &= H_0/\hbar - \Big(\sum_{i,l}\Omega^{\rm R}_{e_ig_l}|e_i\rangle\langle g_l| \\ &\quad +\sum_i \Omega^{\rm R}_{e_id}|e_i\rangle\langle d| + {\rm c.c}\Big) + H_m/\hbar, \\ H_0/\hbar &= \sum_i \omega_{e_i}|e_i\rangle\langle e_i| + \sum_l \omega_{g_l}|g_l\rangle\langle g_l| + \omega_d|d\rangle\langle d|, \\ H_m &= g_S\mu_{\rm B}\hat{S}\cdot\boldsymbol{B}, \end{aligned} \tag{3}$$

where $\hbar=h/2\pi$ (h is Planck's constant), $\Omega^{\rm R}_{e_ig_l}$ and $\Omega^{\rm R}_{e_id}$ are the corresponding Rabi frequencies, $|e_i\rangle$ is the excited state, $|g_l\rangle$ is the ground state, and $|d\rangle$ is another state that includes all other possible vibrational levels as the total population probabilities are equal to 1. g_S is the electron g-factor and $\mu_{\rm B}$ is the Bohr magneton. Assuming that the total decay rate is Γ_i and the decay rate for each channel is Γ_{kl}, the complete density matrix equation of motion for the $M_{\rm g}+M_{\rm e}$ system is given by

$$\begin{aligned} \dot{\rho}_{e_ie_i} &= \sum_m {\rm Im}\left[\Omega^*_{e_ig_m}\tilde{\rho}_{e_ig_m}\right] + {\rm Im}\left[\Omega^*_{e_id}\tilde{\rho}_{e_id}\right] - \Gamma_i\rho_{e_ie_i}, \\ \dot{\rho}_{e_ie_j} &= \frac{\rm i}{2}\Big[2\left(\omega_{e_j}-\omega_{e_i}\right)\rho_{e_ie_j} \\ &\quad -\sum_m\left(\Omega^*_{e_jg_m}\tilde{\rho}_{e_ig_m}-\Omega_{e_ig_m}\tilde{\rho}^*_{e_jg_m}\right) \\ &\quad -\left(\Omega^*_{e_jd}\tilde{\rho}_{e_id}-\Omega_{e_id}\tilde{\rho}^*_{e_jd}\right)\Big] - \frac{\Gamma_i+\Gamma_j}{2}\rho_{e_ie_j}, \\ \dot{\tilde{\rho}}_{e_id} &= \frac{\rm i}{2}\Big[2\left(\omega^{\rm L}_{ed}+\omega_d-\omega_{e_i}\right)\tilde{\rho}_{e_id} - \Omega_{e_id}\left(\rho_{e_ie_i}-\rho_{dd}\right) \\ &\quad +\sum_m\Omega_{e_ig_m}\tilde{\rho}^*_{dg_m} - \sum_{k\neq i}\Omega_{e_kd}\rho_{e_ie_k}\Big] - \frac{\Gamma_i}{2}\tilde{\rho}_{e_id}, \\ \dot{\tilde{\rho}}_{e_ig_l} &= \frac{\rm i}{2}\Big[2\left(\omega^{\rm L}_{eg}+\omega_{g_l}-\omega_{e_i}\right)\tilde{\rho}_{e_ig_l} - \Omega_{e_ig_l}\left(\rho_{e_ie_i}-\rho_{g_lg_l}\right) \\ &\quad +\sum_{m\neq l}\Omega_{e_ig_m}\rho_{g_mg_l} \\ &\quad -\sum_{k\neq i}\Omega_{e_kg_l}\rho_{e_ie_k}+\Omega_{e_id}\tilde{\rho}_{dg_l}\Big] - \frac{\Gamma_i}{2}\tilde{\rho}_{e_ig_l}, \\ \dot{\rho}_{dd} &= -\sum_k\dot{\rho}_{e_ke_k} - \sum_m\dot{\rho}_{g_mg_m}, \\ \dot{\tilde{\rho}}_{dg_l} &= \frac{\rm i}{2}\Big[2\left(\omega^{\rm L}_{eg}+\omega_{g_l}-\omega^{\rm L}_{ed}-\omega_d\right)\tilde{\rho}_{dg_l} \\ &\quad -\sum_k\left(\Omega_{e_kg_l}\tilde{\rho}^*_{e_kd}-\Omega^*_{e_kd}\tilde{\rho}_{e_kg_l}\right)\Big], \\ \dot{\rho}_{g_lg_l} &= \sum_k\left(-{\rm Im}\left[\Omega^*_{e_kg_l}\tilde{\rho}_{e_kg_l}\right]+\Gamma_{kl}\rho_{e_ke_k}\right), \\ \dot{\rho}_{g_lg_n} &= \frac{\rm i}{2}\Big[2\left(\omega_{g_n}-\omega_{g_l}\right)\rho_{g_lg_n} \\ &\quad -\sum_k\left(\Omega_{e_kg_n}\tilde{\rho}^*_{e_kg_l}-\Omega^*_{e_kg_l}\tilde{\rho}_{e_kg_n}\right)\Big], \\ \tilde{\rho}_{e_ig_l} &\equiv \rho_{e_ig_l}\,{\rm e}^{{\rm i}\omega^{\rm L}_{eg}t}, \\ \tilde{\rho}_{e_id} &\equiv \rho_{e_id}\,{\rm e}^{{\rm i}\omega^{\rm L}_{ed}t}, \\ \tilde{\rho}_{dg_l} &\equiv \rho_{dg_l}\,{\rm e}^{{\rm i}\left(\omega^{\rm L}_{eg}-\omega^{\rm L}_{ed}\right)t}. \end{aligned} \tag{4}$$

According to the studies from Liebisch *et al.* in 2012, the bichromatic light ensures efficient slowing since the $F_{\rm g}=2\rightarrow F_{\rm e}=3$ cycling transition provides a nearly ideal two-level system.[48] The model of Rb atoms is based on numerical solutions of the optical Bloch equations for two-level atoms driven by multiple time-dependent fields:

$$\begin{aligned} \dot{\rho}_{gg} &= \frac{\rm i}{\hbar}\left(\rho_{eg}-\rho_{ge}\right)dE+\gamma\rho_{ee}, \\ \dot{\rho}_{ge} &= \frac{\rm i}{\hbar}\left(\rho_{ee}-\rho_{gg}\right)dE+\left({\rm i}\omega_{\rm a}-\frac{\gamma}{2}\right)\rho_{ge}, \\ \rho_{ge} &= \rho^*_{eg}, \quad \rho_{gg}+\rho_{ee}=1, \end{aligned} \tag{5}$$

where d is the matrix element of the electric dipole moment, E is the magnitude of the electric field, and γ is the scattering rate of the excited state for the atom.

The force acting on a molecule or an atom is equal to the negative gradient of the interaction potential, which is given by

$$\langle\hat{F}\rangle = -\langle\nabla\hat{H}\rangle = -{\rm Tr}\left(\rho\nabla\hat{H}\right). \tag{6}$$

2.2. Scheme of dual-species stimulated deceleration

A proposed scheme is shown in Fig. 2: atomic and molecular beams (blue) emerge from the buffer gas chamber, where the particle density typically ranges from 10^{13} cm^{-3} to 10^{14} cm^{-3} in cell, and the temperature is usually around 4 K.[50–52] The upper right part of the figure shows the expected temperature (T) and velocity (V) variations of the atoms and molecules. Initially, the atoms and molecules move at high velocities (typically a few hundred m/s). Due to expansion, diffusion, and collisions with the buffer gas, their density decreases rapidly. Deceleration needs to be carried out in the moving reference frame to ensure sufficient interaction between the particles and the laser. The laser beam frequency along the z-direction is chirped in the moving reference frame to achieve deceleration. In the moving reference frame, two sets of laser fields are applied to the atoms and molecules for dual-species stimulated deceleration. The red arrows represent the 780-nm laser for decelerating Rb atoms, and the purple arrows represent the 359-nm laser for decelerating MgF molecules. To realize the deceleration process of MgF molecules, the main cooling laser operates at a wavelength of 359 nm, while the repumping laser has a wavelength of 368 nm. These required ultraviolet wavelengths can be achieved by frequency doubling the fundamental light generated by a titanium-sapphire laser, which meets the laser power requirements. The black arrows represent the MOT. The two counter-propagating travelling-wave lights of 359 nm are linearly polarized driving the transition of $X^2\Sigma_{1/2}(v=0,N=1)\rightarrow A^2\Pi_{1/2}(v'=0,J'=1/2)$, and interact with MgF molecules at a uniform magnetic field. This type of transition will lead to optical pumping into dark ground-state Zeeman sublevels, which could not be excited by the lasers. The states of $F=2$, $m=\pm2$ in the ground state $X^2\Sigma_{1/2}(v=0,N=1)$ are the dark states for MgF. Once there is a dark state, the ground molecular hyperfine state is no longer coupled to the excited state by the cooling laser, and the cooling will cease. Applying a magnetic field induces the Larmor precession of the molecules, which leads to a periodic exchange of populations of the ground states, so that the molecule will not be trapped in the dark state. Note that the Larmor precession effect is closely associated with the magnitude of the magnetic field and the angle with the direction of polarized light. The magnitude of the magnetic field is 25 Gs (1 Gs = 10^{-4} T), and the angle with the direction of polarized light is 65°.

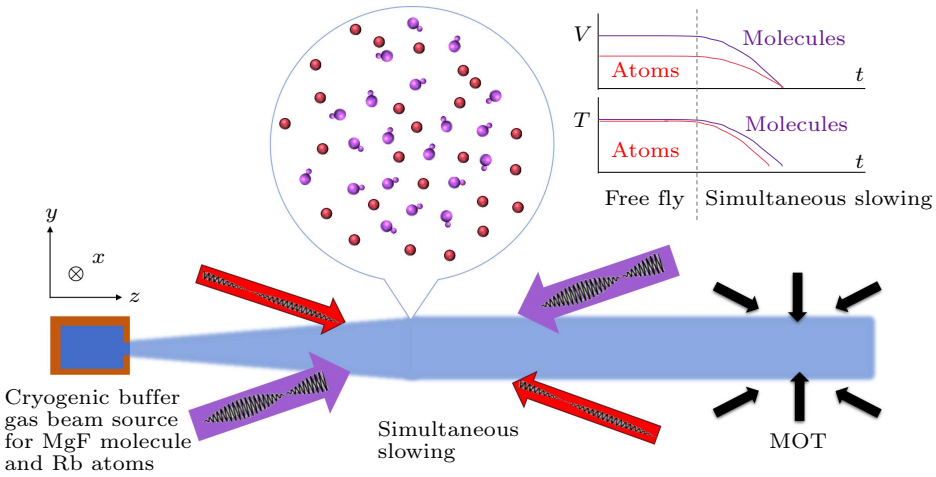


Fig. 2. Proposed scheme of dual-species stimulated deceleration of MgF molecules with Rb atoms. A beam (in blue) of atoms and molecules is extracted from the buffer gas chamber (brown box). The upper right part of the figure shows the expected temperature (T) and velocity (V) variations for the atoms and molecules. In the moving reference frame, two sets of laser fields are applied to the atoms and molecules for dual-species stimulated deceleration. The red arrows represent the 780-nm laser for decelerating Rb atoms, and the purple arrows represent the 359-nm laser for decelerating MgF molecules. Slowing and cooling can be achieved in the moving reference frame by tuning the frequency of the cooling laser. Not all lasers are shown in the figure.

Stimulated forces rely on the coherent control of momentum exchange through rapid absorption-stimulated emission cycles, producing a large net force with appropriate laser power and sequencing. The magnitude and the velocity capture range of stimulated forces is also more favourable than that of spontaneous radiation forces.[26,53] The magnitude of the velocity-dependent force decreases significantly as the beat phase difference increases, which occurs when the molecular beam travels a short distance of several centimetres, and the phase compensation allows an optimal shape for the stimulated force to be maintained.[30,54] However, since the stimulated force is sizable only for velocities within the range of $|v|<\delta/2k$ and the velocity distribution of the decelerated molecules is typically broad, the effective deceleration forces are unevenly distributed throughout the slowing process.[54,55] Meanwhile, the magnitude of the stimulated force acting on molecules increases with δ; however, the required laser power scales with δ^2.[30,55] The tightly focused laser beams with a top-hat diameter of 1 mm are used to achieve the required irradiance.[28] Note that requiring the high-power laser light

presents a significant challenge in actual experiments, especially when the detuning is several hundred times the natural linewidth γ. These issues greatly hinder laser deceleration efficiency and ultimately decrease the number of slowed molecules. Therefore, the dual-species deceleration of MgF molecules with Rb atoms by stimulated force with a phase compensation and frequency chirping can effectively address issues related to high laser power requirements and spatial inhomogeneity of stimulated forces on molecules during deceleration. The lasers have a detuning of $-\delta$ from atomic resonance ω_a and is shifted to $\omega_a \pm \delta$ using an acousto-optic modulator. These beams are combined by a polarizing beam splitter and further split by a beam splitter. The frequency is chirped via electro-optic modulator driven by a voltage-controlled oscillator modulated with a sawtooth input to achieve synchronous deceleration and compensation for Doppler shifts.[54] The chirping rate can be precisely controlled. Then, one laser beam with the frequency of $\omega_a \pm \delta + kv(t)$ will be a blue-tuned one after an optical delay line to adjust the relative beat phase, and the other will become a red-tuned beat note train. The leg-coated prism mirrors from Thorlabs can be used to create an optical delay line. The phase change could be adjusted by synchronizing the position of the optical delay line with the motion of molecules using stepper motors.[30,54]

3. Results and discussion

3.1. Stimulated forces with a phase compensation

The beat phase difference strongly influences the magnitude of the stimulated force. Initially, the molecules and atoms are in their ground state. When they interact with the light pulse, stimulated emission occurs, releasing a photon at the frequency of the absorbed light. If the molecules and atoms have spontaneously returned to the ground state before the counterpropagating beat arrives, they will absorb photons from the opposite direction. This results in a change in the absorption-stimulated radiation cycles and reverses the direction of the stimulated forces. In this case, the deceleration process would transition into an acceleration process. Thus, the average stimulated force is zero if the π pulses in opposite directions are evenly distributed in time.[53] Therefore, controlling the beat phase difference is crucial for maintaining the optimal stimulated force profile on molecules and atoms during deceleration. The particles can be decelerated by maintaining a constant beat phase difference through an optical phase compensation method, ensuring the sustained application of a favourable force throughout the deceleration process.[30,54] Through the calculation of the relationship between Ω^0 and the velocity-averaged stimulated force in the two-level systems, the optimal Rabi frequency amplitude Ω^0 is determined to be $\sqrt{3/2}\delta$.[54,55]

We have investigated the stimulated force on MgF molecules as the beat phase difference (φ) varies from 90° to 165°. As shown in Fig. 3(a), when $\varphi = 90°$, the magnitude of the stimulated force for MgF molecules is about $1.1hk\gamma/4\pi$ and the velocity capture range of $\delta/2k$ is 35.7 m/s. As the phase difference increases to 135°, the magnitude of the stimulated force decreases to $0.3hk\gamma/4\pi$, as shown in Fig. 3(d). Meanwhile, the characteristic "hat-shaped" profile of the force gradually disappears. As φ continues to increase, the stimulated force acting on MgF molecules gradually decreases. And, as shown in Figs. 3(e) and 3(f), the force within the effective velocity range approaches zero. Therefore, modulating the phase difference during the deceleration process is crucial. An optical phase compensation method can maintain an optimal force profile throughout the deceleration. Overall, the stimulated force features a large magnitude and a wide velocity range with the phase difference of $\varphi = 90°$.

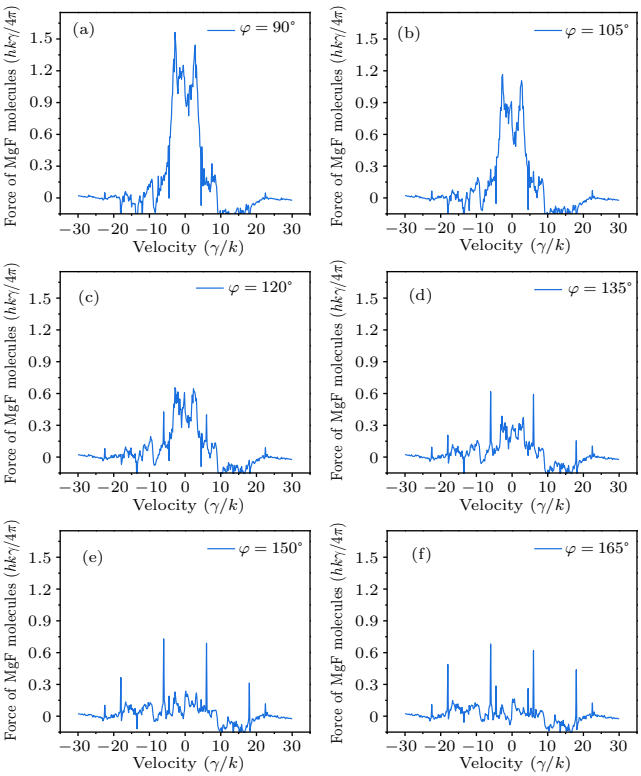


Fig. 3. Stimulated force on MgF molecules as the beat phase difference (φ) varies from 90° to 165°. The blue curves represent the force on MgF molecules with the magnetic field of $B = 25$ Gs and $\theta = 65°$, for δ values of 9γ.

Figure 4 shows the stimulated forces on MgF molecules and Rb atoms. The constant beat phase difference (φ) is 90°. The blue curve represents the force on MgF molecules with the magnetic field of $B = 25$ Gs and $\theta = 65°$. For δ values of 9γ, the velocity capture range of $\delta/2k$ is 35.7 m/s at a laser power of 357 mW per traveling wave. The magnitude of the stimulated force for MgF molecules is about $1.1hk\gamma/4\pi$. The red curve represents the force on Rb atoms at $\delta = 8\gamma$ with the velocity capture range of 18.7 m/s, and the stimulated force

is $1.3hk\gamma/4\pi$, at a laser power of 10 mW per traveling wave (40 mW in total).

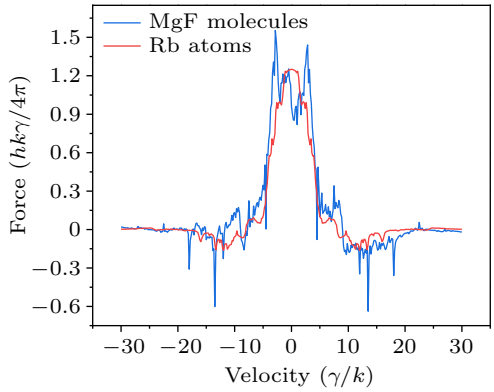


Fig. 4. The stimulated force on MgF molecules and Rb atoms. The blue curve represents the force on MgF molecules with the magnetic field of $B = 25$ Gs and $\theta = 65°$. For δ values of 9γ, the velocity capture range of $\delta/2k$ is 35.7 m/s. The red curve represents the force on Rb atoms at $\delta = 8\gamma$ with the velocity capture range of 18.7 m/s.

3.2. Relationship between the deceleration effect and the chirping process

The frequency chirping method ensures a constant maximum stimulated force on the MgF and Rb during the deceleration process, allowing for a sustained interaction between the moving particles and the low-power light.[54] Figure 5 shows the trend in the number of atoms and molecules with velocities below 10 m/s as the duration of the chirp ramp (Δt) varies. The chirp rate is defined as the ratio of the chirp magnitude to the duration of the chirp ramp ($\Delta\omega/\Delta$t), and the chirp magnitude varies with the initial longitudinal velocity of the atoms and molecules. The MgF molecular beam from a buffer gas source has a forward velocity distribution centred at 200 m/s with a full width at half maximum (FWHM) of 100 m/s. The FWHM of the transverse velocity distribution is fixed at 2 m/s after the molecules pass through the collimation aperture.[56] The Rb atomic beam from a buffer gas source is assumed to have a forward velocity of 130 m/s with an FWHM of 80 m/s and a transverse velocity distribution with an FWHM of 2 m/s.[51] The chirp magnitude is 557 MHz for MgF molecules and 141 MHz for Rb atoms.[26] We perform the Monte Carlo simulations for the deceleration process for 10^6 Rb atoms and 10^6 MgF molecules. We count the number of the atoms and molecules with velocities below 10 m/s in the detection range. The fraction is expressed by dividing the number of the slowed molecules by the initial one million. Thus, the final number of detected particles is lower than the initial number due to transverse diffusion during deceleration. As shown in Fig. 5(a), the blue curve represents the change in the number of MgF molecules with velocities below 10 m/s as the duration of the chirp ramp (Δt) varies from 0.5 ms to 2.5 ms. When the Δt is 1 ms (the chirp rate is 557 MHz/ms), the fraction of the slow MgF molecules is maximized at 26%. As the duration continues to increase, the fraction of slow MgF molecules decreases rapidly. For $\Delta t = 2.5$ ms, the fraction is 8%. When $\Delta t = 1$ ms, the fraction is 3.25 times that of $\Delta t = 2.5$ ms. As shown by the red curve in Fig. 5(b), the fraction of Rb atoms below 10 m/s is maximized at 14% when the duration of the chirp ramp is 1 ms (the chirp rate is 141 MHz/ms). When Δt is 0.6 ms, the fraction of the slow Rb atoms is only 2%, which is about one-seventh of the fraction observed at $\Delta t = 1$ ms. As a result, the optimal chirp rate is 557 MHz/ms for MgF molecules and 141 MHz/ms for Rb atoms, at a laser power of 357 mW (MgF) and 10 mW (Rb) per traveling wave.

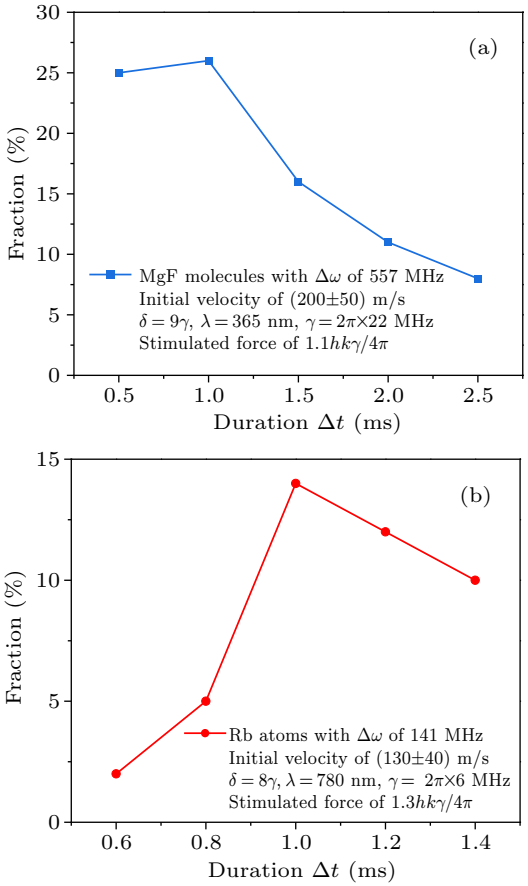


Fig. 5. The trend in the number of (a) MgF molecules ($\delta = 9\gamma$) and (b) Rb atoms ($\delta = 8\gamma$) with velocities below 10 m/s as the duration of the chirp ramp (Δt) varies. The fraction is expressed as the number of slowed particles divided by the initial million. The chirp magnitude is 557 MHz (MgF) and 141 MHz (Rb).

3.3. Monte Carlo simulation of the deceleration dynamics process

Figure 6 shows the results of the dual-species stimulated deceleration of MgF molecules ($\delta = 9\gamma$, chirp rate is 557 MHz/ms) with Rb atoms ($\delta = 8\gamma$, chirp rate is 141 MHz/ms). As shown in Fig. 6(a), the MgF molecular beam has an initial $v = (200 \pm 50)$ m/s. After 1 ms of deceleration, about 2.6×10^5 MgF molecules have the velocities of about 8 m/s. Meanwhile, the Rb atoms are simultaneously decelerated to the velocity below 5 m/s, with the number of 1.4×10^5 Rb atoms, as shown in Fig. 6(b). During the deceleration process, some Rb atoms and still exhibit relatively

high velocities, about above 150 m/s. For MgF molecules, due to their higher velocities, the molecules quickly leave the detection range, resulting in a relatively smaller number of high-speed MgF molecules being detected. The change in the width of the molecular velocity distribution during deceleration indicates that the stimulated force not only effectively reduces the molecular velocity, but also narrows the distribution of longitudinal velocities, thus providing a cooling effect. As shown by the orange and yellow curves in Figs. 6(a) and 6(b), compared with Rb atoms, the longitudinal velocity distribution of MgF molecules is compressed earlier, resulting in a faster temperature reduction.

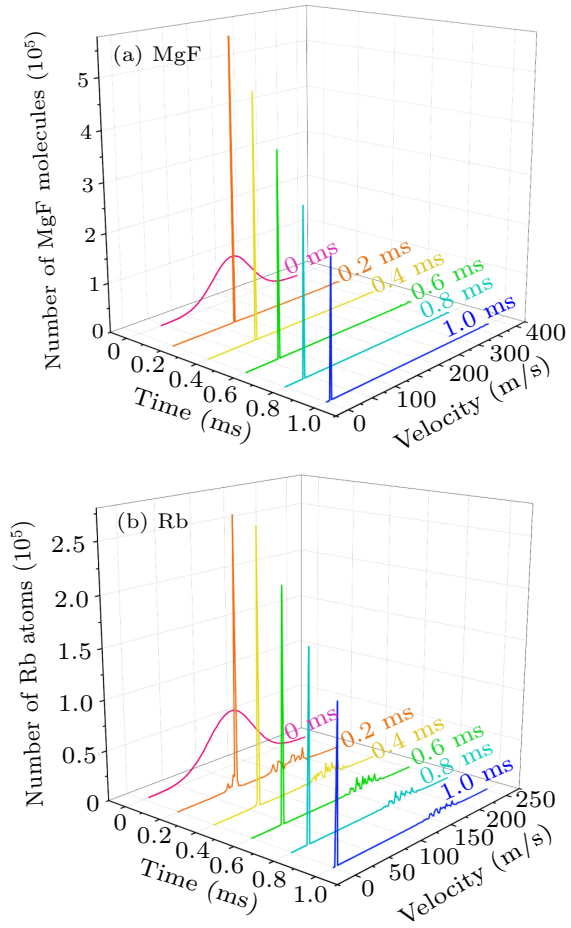


Fig. 6. The dual-species stimulated deceleration of (a) MgF molecules ($\delta = 9\gamma$) with (b) Rb atoms ($\delta = 8\gamma$). The MgF beam has an initial $v = (200 \pm 50)$ m/s, and the Rb beam has an initial $v = (130 \pm 40)$ m/s. The chirp rate is 557 MHz/ms for MgF molecules and 141 MHz/ms for Rb atoms. The initial number of MgF molecules and Rb atoms is 10^6, respectively.

The reduction in the number of particles during the deceleration process indicates a loss of particles. Although the time of stimulated deceleration is short, the loss due to transverse diffusion remains significant. We examine the variation of the transverse particle beam size during deceleration for different initial transverse velocities, as shown in Fig. 7. The lines with triangular markers represent the initial transverse velocity of 5 m/s and the blue lines with circular markers represent the initial transverse velocity of 1 m/s. The red line shows the transverse beam size of the MgF molecular beam and the blue line shows the transverse beam size of the Rb atomic beam. When the initial transverse velocity is 1 m/s, the transverse beam size of the MgF molecules increases from 1.67 mm to 2.95 mm, as shown in Fig. 7(a). However, when the initial transverse velocity is 5 m/s, the transverse beam size of the MgF molecules increases rapidly from 3.81 mm to 12.55 mm. As the deceleration time increases from 0.1 ms to 1 ms, the molecular size increases by about a factor of 3.3. From Fig. 7(b), the red line with circular markers shows that the transverse beam size of the Rb atoms increases from 1.83 mm to 3.21 mm, an increase of 1.38 mm. When the initial transverse velocity is 5 m/s, the atomic transverse beam size has an increase of 8.94 mm, from 4.93 mm to 13.87 mm. Compared to the case with an initial transverse velocity of 1 m/s, the increase is 6.5 times larger. Therefore, during the deceleration process with stimulated radiation force, the loss due to transverse diffusion cannot be ignored, and it is crucial to minimize the transverse velocity of the particles as much as possible.

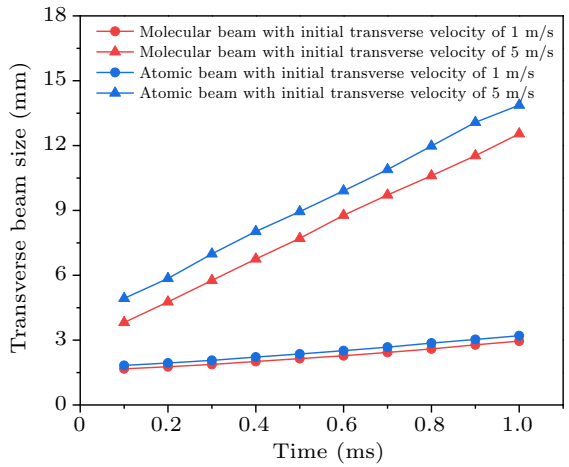


Fig. 7. The variation of the transverse beam size during the dual-species stimulated deceleration for (a) MgF molecules ($\delta = 9\gamma$) and (b) Rb atoms ($\delta = 8\gamma$). The lines with triangular markers represent the initial transverse velocity of 5 m/s and the blue lines with circular markers represent the initial transverse velocity of 1 m/s. The red line shows the transverse beam size of the MgF molecular beam and the blue line shows the transverse beam size of the Rb atomic beam.

To investigate the deceleration dynamics of all molecules, we analyze the velocity distribution and flight times of one million molecules after deceleration. As shown in Fig. 8(a), most of the orange dots are concentrated around 8 m/s to 8.2 m/s, with a few scattered between 8.3 m/s and 8.6 m/s. This indicates that the width of the longitudinal velocity distribution after deceleration is about 0.2 m/s, which is much smaller than the initial velocity distribution width of 100 m/s, resulting in efficient cooling. Most of the MgF molecules experience a deceleration distance ranging from 1.2 cm to 2.1 cm. Figure 8(b) shows that the slow molecules arrive at the MOT position within 2 ms. At a flight time of about 1.2 ms, many faster molecules are observed and their velocity distribution is quite broad. As the deceleration pro-

gresses, when the flight time exceeds 1.5 ms, the number of slow molecules increases, and the velocity distribution becomes significantly narrower, as indicated by the purple dots in Fig. 8(b). The extremely short deceleration time significantly minimizes the loss of the molecules due to transverse diffusion during flight. The exit aperture of the buffer gas cell is 3 mm–5 mm in diameter to extract a precooled molecular beam, and a 1.5 mm×1.5 mm aperture is used to further collimate the molecular beam for deceleration and cooling,[50] resulting in a steradian of 1.9×10^{-4}.[56] If the flux of MgF from a buffer gas chamber is $\sim10^{11}$ per steradian per molecular pulse in the ground state,[41,57] we can estimate the number of slowed MgF molecules that satisfy a typical MOT capture velocity range.[57] The spatial distribution of molecules within 1 cm after deceleration indicates that about $\sim 9.0\times10^{6}$ MgF molecules can be confined in the MOT, which is about an order of magnitude higher than the number of molecules decelerated by spontaneous radiation force.[26]

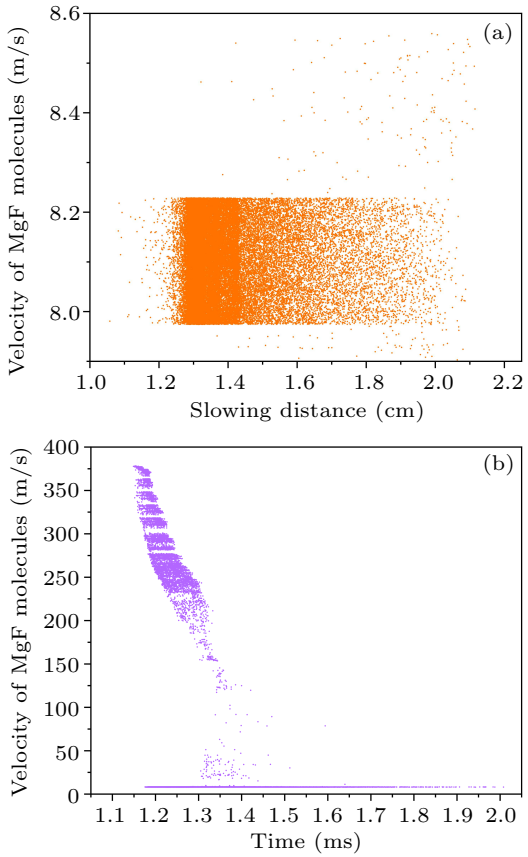


Fig. 8. Velocity distribution and flight times of one million molecules after deceleration. (a) Longitudinal velocity distribution of MgF molecules with slowing distance after laser slowing is completed, shown by the orange dots. (b) Flight time and forward velocity of MgF molecules reaching the MOT position, shown by the purple dots.

4. Conclusion

In conclusion, we have presented a new approach to obtain cold atom–molecule mixtures to enable effective dual-species slowing of atoms and molecules, applicable to species that can be laser-cooled, including atoms and many molecular radicals. Theoretical studies indicate that MgF molecules and Rb atoms can be simultaneously decelerated to an MOT capture velocity range, eliminating nearly 99% of their kinetic energy, at a laser power of only 357 mW (MgF) and 10 mW (Rb) per traveling wave. The short deceleration time minimizes molecular loss due to transverse diffusion during the flight. Compared to Rb atoms, the longitudinal velocity distribution of MgF molecules is compressed earlier, resulting in a faster temperature reduction. The longitudinal velocity distribution widths of the MgF molecules before and after deceleration are 100 m/s and 0.2 m/s, respectively, resulting in efficient cooling. The estimated number of molecules that can be confined in an MOT is 9.0×10^{6}, which is about an order of magnitude higher than the number of molecules decelerated by spontaneous radiation force.[26] This scheme enhances the deceleration efficiency of atoms and molecules to the MOT confinement velocity and promotes a higher spatial overlap between atoms and molecules, which not only provides a basis for studying the Bose–Einstein condensation of MgF molecules, but also provides a starting point for further exploration of sympathetic cooling and atom–molecule collisions in the ultra-low temperature regime.[38]

Acknowledgement

Project supported by the National Natural Science Foundation of China (Grant Nos. 12174115 and 91836103).

References

[1] DeMille D, Doyle J M and Sushkov A O 2017 *Science* **357** 990
[2] Anderegg L, Vilas N B, Hallas C, Robichaud P, Jadbabaie A, Doyle J M and Hutzler N R 2023 *Science* **382** 665
[3] DeMille D, Hutzler N R, Rey A M and Zelevinsky T 2024 *Nat. Phys.* **20** 741
[4] Carr L D, DeMille D, Krems R V and Ye J 2009 *New J. Phys.* **11** 055049
[5] Karman T, Tomza M and Pérez-Ríos J 2024 *Nat. Phys.* **20** 722
[6] Ruttley D K, Hepworth T R, Guttridge A and Cornish S L 2025 *Nature* **637** 827
[7] Holland C M, Lu Y and Cheuk L W 2023 *Science* **382** 1143
[8] Bao Y C, Yu S S, Anderegg L, Chae E, Ketterle W, Ni K K and Doyle J M 2023 *Science* **382** 1138
[9] Langen T, Valtolina G, Wang D and Ye J 2024 *Nat. Phys.* **20** 702
[10] Barry J F, McCarron D J, Norrgard E B, Steinecker M H and DeMille D 2014 *Nature* **512** 286
[11] Anderegg L, Augenbraun B L, Chae E, Hemmerling B, Hutzler N R, Ravi A, Collopy A, Ye J, Ketterle W and Doyle J M 2017 *Phys. Rev. Lett.* **119** 103201
[12] Truppe S, Williams H J, Hambach M, Caldwell L, Fitch N J, Hinds E A, Sauer B E and Tarbutt M R 2017 *Nat. Phys.* **13** 1173
[13] Collopy A L, Ding S, Wu Y, Finneran I A, Anderegg L, Augenbraun B L, Doyle J M and Ye J 2018 *Phys. Rev. Lett.* **121** 213201
[14] Zeng Z X, Deng S H, Yang S K and Yan B 2024 *Phys. Rev. Lett.* **133** 143404
[15] Vilas N B, Hallas C, Anderegg L, Robichaud P, Winnicki A, Mitra D and Doyle J M 2022 *Nature* **606** 70
[16] Anderegg L, Augenbraun B L, Bao Y C, Burchesky S, Cheuk L W, Ketterle W and Doyle J M 2018 *Nat. Phys.* **14** 890

[17] McCarron D J, Steinecker M H, Zhu Y and DeMille D 2018 *Phys. Rev. Lett.* **121** 013202

[18] Williams H J, Caldwell L, Fitch N J, Truppe S, Rodewald J, Hinds E A, Sauer B E and Tarbutt M R 2018 *Phys. Rev. Lett.* **120** 163201

[19] Anderegg L, Cheuk L W, Bao Y C, Burchesky S, Ketterle W, Ni K K and Doyle J M 2019 *Science* **365** 1156

[20] Barry J F, Shuman E S, Norrgard E B and DeMille D 2012 *Phys. Rev. Lett.* **108** 103002

[21] Hemmerling B, Chae E, Ravi A, Anderegg L, Drayna G K, Hutzler N R, Collopy A L, Ye J, Ketterle W and Doyle J M 2016 *J. Phys. B* **49** 174001

[22] Truppe S, Williams H J, Fitch N J, Hambach M, Wall T E, Hinds E A, Sauer B E and Tarbutt M R 2017 *New J. Phys.* **19** 022001

[23] Yeo M, Hummon M T, Collopy A L, Yan B, Hemmerling B, Chae E, Doyle J M and Ye J 2015 *Phys. Rev. Lett.* **114** 223003

[24] Kaebert P, Stepanova M, Poll T, Petzold M, Xu S, Siercke M and Ospelkaus S 2021 *New J. Phys.* **23** 093013

[25] Rodriguez K J, Pilgram N H, Barker D S, Eckel S P and Norrgard E B 2023 *Phys. Rev. A* **108** 033105

[26] Yan K, Gu R X, Wu D, Wei J, Xia Y and Yin J P 2022 *Front. Phys.* **17** 42502

[27] Metcalf H 2017 *Rev. Mod. Phys.* **89** 041001

[28] Galica S E, Aldridge L, McCarron D J, Eyler E E and Gould P L 2018 *Phys. Rev. A* **98** 023408

[29] Kozyryev I, Baum L, Aldridge L, Yu P, Eyler E E and Doyle J M 2018 *Phys. Rev. Lett.* **120** 063205

[30] Yin Y N, Xu S P, Xia M, Xia Y and Yin J P 2018 *Phys. Rev. A* **97** 043403

[31] Marsman A, Horbatsch M and Hessels E A 2023 *Phys. Rev. A* **108** 012811

[32] Wallis A O G and Hutson J M 2009 *Phys. Rev. Lett.* **103** 183201

[33] Lim J, Frye M D, Hutson J M and Tarbutt M R 2015 *Phys. Rev. A* **92** 053419

[34] Akerman N, Karpov M, Segev Y, *et al.* 2017 *Phys. Rev. Lett.* **119** 073204

[35] Morita M, Kosicki M B, Żuchowski P S, *et al.* 2018 *Phys. Rev. A* **98** 042702

[36] Liu Y and Luo L 2021 *Front. Phys.* **16** 12504

[37] Zhu Y 2021 *Experiments with* ^{87}*Rb: Towards Co-trapping* $^{88}Sr^{19}F$ *and* ^{87}*Rb* Ph.D. Dissertation (Yale University)

[38] Zhang C, Rittenhouse S T, Tscherbul T V, *et al.* 2024 *Phys. Rev. Lett.* **132** 033001

[39] Rodriguez K J, Pilgram N H, Barker D S, Eckel S P and Norrgard E B 2023 *Phys. Rev. A* **108** 033105

[40] Pilgram N H, Baldwin B W, La Mantia D S, Eckel S P and Norrgard E B 2024 *Phys. Rev. A* **110** 023110

[41] Wu D, Yan K, Wei J, Dong T J, Xia Y and Yin J P 2025 *Front. Phys.* **20** 032201

[42] Chae E 2021 *Phys. Chem. Chem. Phys.* **23** 1215

[43] Xu S, Xia M, Gu R X, Yin Y N, Xu L, Xia Y and Yin J P 2019 *Phys. Rev. A* **99** 033408

[44] Yan K, Wei B, Yin Y L, Xu S, Xu L, Xia M, Gu R X, Xia Y and Yin J P 2020 *New J. Phys.* **22** 033003

[45] Xia M, Gu R X, Yan K, Wu D, Xu L, Xia Y and Yin J P 2021 *Phys. Rev. A* **103** 013321

[46] Gu R X, Yan K, Wu D, Wei J, Xia Y and Yin J P 2022 *Phys. Rev. A* **105** 042806

[47] Aldridge L, Galica S E and Eyler E E 2016 *Phys. Rev. A* **93** 013419

[48] Liebisch T C, Blanshan E, Donley E A and Kitching J 2012 *Phys. Rev. A* **85** 013407

[49] Anderson M H, Ensher J R, Matthews M R, *et al.* 1995 *Science* **269** 198

[50] Hofsäss S, Doppelbauer M, Wright S C, Kray S, Sartakov B G, Pérez-Ríos J, Meijer G and Truppe S 2021 *New J. Phys.* **23** 075001

[51] Hutzler N R, Lu H I and Doyle J M 2012 *Chem. Rev.* **112** 4803

[52] Wright S C, Doppelbauer M, Hofsäss S, Schewe H C, Sartakov B, Meijer G and Truppe S 2023 *Mol. Phys.* **121** e2146541

[53] Galica S E, Aldridge L and Eyler E E 2013 *Phys. Rev. A* **88** 043418

[54] Wei J, Wu D, Dong T J, Zu C Y, Xia Y and Yin J P 2025 *Phys. Rev. A* **111** 013307

[55] Chieda M A and Eyler E E 2012 *Phys. Rev. A* **86** 053415

[56] Shuman E S, Barry J F and DeMille D 2010 *Nature* **467** 820

[57] Williams H J, Truppe S, Hambach M, Caldwell L, Fitch N J, Hinds E A, Sauer B E and Tarbutt M R 2017 *New J. Phys.* **19** 113035